

Photovoltaic Devices Using Sublimed Methylammonium Lead Iodide Perovskites: Long-Term Reproducible Processing

Kassio P. S. Zanoni,* Lucia Martínez-Goyeneche, Chris Dreessen, Michele Sessolo, and Henk J. Bolink*

Fully evaporated solar cells using methylammonium iodide (MAI)-based perovskites can reach power conversion efficiencies exceeding 20%. An important point to advance perovskite photovoltaics is to ensure reproducibility from batch to batch. Sublimation control of organic ammonium halides is critical in achieving this for evaporated perovskite solar cells. Herein, a reproducible procedure for the coevaporation of PbI_2 and MAI based on an evaporator chamber setup with only two quartz crystal microbalances (QCMs) is described. One QCM monitors exclusively the PbI_2 precursor (PbI_2 -QCM) and the second QCM monitors the total amount of MAPbI_3 mass reaching the substrates (MAPbI_3 -QCM). It is shown that the MAI evaporation can be reliably monitored, indirectly, through the MAPbI_3 -QCM. In this way, the fluctuating sublimation rates usually observed due to variations of MAI purity are avoided. This allows one to obtain consistently high-performing solar cells over a period of one and a half years.

1. Introduction


Perovskite solar cells (PSCs) are viable sources of efficient and affordable energy that has attracted much interest since their onset in 2009 due to rapidly increasing device power conversion efficiencies (PCEs, currently above 25.6% already).^[1] High-quality (poly-)crystalline perovskite films have a combination of desirable properties, mainly high absorption coefficient, high ambipolar charge mobility, and long charge carrier diffusion length.^[2] These properties are directly related to the film morphology, stoichiometry, and density of defects in the bulk or at the surface. Hence, to ensure reproducible preparation of

PSCs, it is crucial that the perovskite growth during deposition is controllable in a repeatable way independent of batch-to-batch purity variations of the precursor salts used. A stable reproducible baseline cell performance is crucial to advance the technology and further optimize the efficiency and stability. Numerous deposition processes are investigated, from solvent-based techniques such as spin coating, blade coating, and solvent engineering to vacuum-based methods, such as thermal vacuum deposition or close space sublimation or even hybrid sequential depositions.^[2–11] Physical vapor deposition (PVD) is a very versatile technique that can be used to grow films of many classes of materials, such as metallic, semiconducting, and insulating films for use in photovoltaics

and light-emitting devices, as well as resistors, transparent conductive oxides, corrosion resistant coatings, magnetic films, among many others. This technique is widely used in the optoelectronic/semiconductor industry for being compatible with large area and high throughput, granting high purity and uniformity to the deposited films.^[9,12–17] It also allows for the in situ monitoring of the deposition rate using quartz crystal microbalances (QCM), which is important when two precursors are cosublimed and to enable precise thickness control.^[12,18] Many research groups have reported on vacuum-deposited perovskites, showing that efficient fully evaporated solar cells are readily achievable. Different perovskite compositions have been prepared ranging from the archetypal MAPbI_3 , requiring the coevaporation of PbI_2 and $\text{CH}_3\text{NH}_3\text{I}$ (methylammonium iodide, MAI) in only two sources,^[19–35] to more complex multication multihalide structures that require the coevaporation from three or more precursors.^[36–43] There are many examples in the literature of coevaporated MAI-based PSCs with PCEs exceeding 20%.^[22,25,43–46] However, despite these successful demonstrations, the sublimation control of organic ammonium halides remains a critical factor in achieving reproducibility of the perovskite film in vacuum-processed devices.

Many authors have found difficulties in monitoring the MAI sublimation, due to fluctuating deposition rates,^[20,22,29,47–51] or in measuring the thickness of the deposited MAI film, complicating the calibration of the QCM sensor.^[20,29,48] Uncontrollable chamber pressures have also been reported.^[31,32,52] Surface-varied adsorption and thermal decomposition have been proposed

K. P. S. Zanoni, L. Martínez-Goyeneche, C. Dreessen, M. Sessolo, H. J. Bolink
 Instituto de Ciencia Molecular
 Universidad de Valencia
 C/Catedrático J. Beltrán 2, 46980 Paterna, Spain
 E-mail: kassio.zanoni@uv.es; henk.bolink@uv.es

 The ORCID identification number(s) for the author(s) of this article can be found under <https://doi.org/10.1002/solr.202201073>.

© 2023 The Authors. Solar RRL published by Wiley-VCH GmbH. This is an open access article under the terms of the Creative Commons Attribution-NonCommercial-NoDerivs License, which permits use and distribution in any medium, provided the original work is properly cited, the use is non-commercial and no modifications or adaptations are made.

DOI: 10.1002/solr.202201073

as the origins of their unusual sublimation behavior.^[12,18,50,51,53–55] This can be mitigated, somewhat, by changes in the setup, such as changing the direction and/or position of the monitoring QCM^[12,56,57] or by controlling the MAI sublimation through the chamber pressure rather than its deposition rate.^[31,52,58,59] Yet, others report the control through the substrate temperature^[44] or through the addition of in situ monitoring methods.^[29,51,60] Importantly, it has been reported that MAI can contain small amounts of impurities; in particular, hypophosphorous acid (H_3PO_2) and phosphorous acid (H_3PO_3), that are used as stabilizers for hydroiodic acid (HI), can react in the synthesis of MAI from HI and methylamine (MA) to form MAH_2PO_2 and MAH_2PO_3 .^[51,61,62] These impurities have been reported to be beneficial for the crystallization of solution-processed MAPbI_3 .^[61–63] However, in vacuum-processed MA-based perovskites, the sublimation of MAI is highly contingent on the MAH_2PO_2 and MAH_2PO_3 impurities. As summarized by Borchert et al., these impurities play no role in the crystallization of coevaporated MAPbI_3 , yet they can increase the sticking coefficient of MAI to the QCM used to monitor the MAI evaporation, allowing a better deposition rate feedback control.^[51] Moreover, studies with mass spectroscopy identified that the impurities are outgassed at a higher rate than the pace of MAI evaporation,^[51] which is likely to affect the deposition rates of long evaporation runs. More recently, Roß et al. showed that highly pure MAI can undergo decomposition into methylamine and hydrogen iodide, which can diffuse omnidirectionally, while the decomposition rate is lower in impure MAI batches, leading to more directional evaporation.^[18] Also, given that the concentration of such impurities typically varies from one batch of MAI to another (either commercially acquired^[51] or synthesized), controlling the deposition rate with a QCM dedicated exclusively to MAI while expecting reproducibility between different MAI evaporations is not trivial.

In our previous publication, we showed that the deposition rate measured on a QCM positioned at the same height as the substrates corresponds precisely to the sum of both MAI and PbI_2 rates, increasing linearly to progressive increase in either MAI or PbI_2 sublimation.^[12] Therein, we established a simple model describing the growth kinetics of a coevaporated MAPbI_3 on the QCM surface, which is initiated with the deposition of solely PbI_2 on the QCM, followed by the adsorption of MAI on this preformed PbI_2 , followed by MAI diffusion into the PbI_2 film and MAPbI_3 crystallization immediately thereafter.

Here we describe a reproducible procedure for the preparation of coevaporated MAPbI_3 that circumvents all the typical problems related to the sublimation of different MAI batches, in particular related to impurities. For that, based on the applicable conclusions from our previous article,^[12] we consider that the rate readings on a QCM placed at the substrate level are not subjected to changes in the sticking ability of MAI, because on this model MAI never gets to adsorb directly on the QCM's gold surface, but rather on a preformed PbI_2 film.^[12] The necessary evaporator components for our proposed procedure are shown in **Figure 1**, highlighting the presence of only two QCMs, one dedicated to monitoring the evaporation of PbI_2 (PbI_2 -QCM) and the second, at the same height as the substrates, dedicated to monitor the deposition of MAPbI_3 (MAPbI_3 -QCM). It is worth noticing there is no QCM dedicated exclusively to MAI, as the MAI evaporation can be monitored indirectly through MAPbI_3 -QCM.

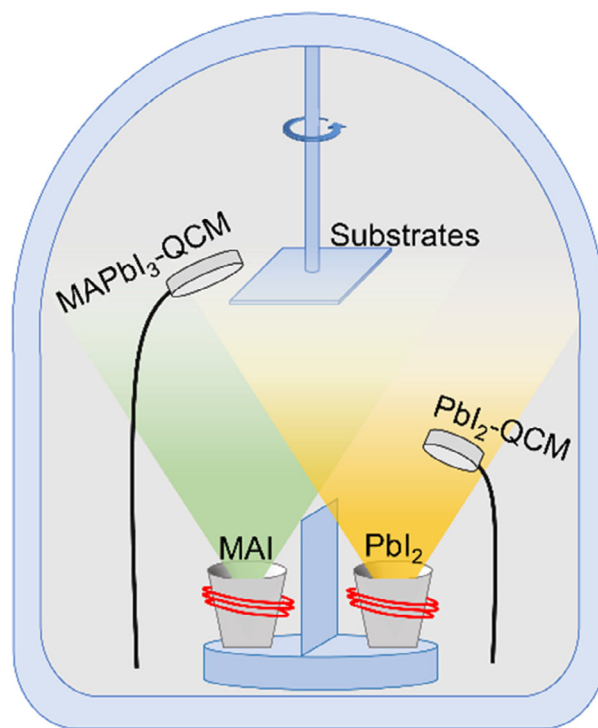


Figure 1. Schematics of the experimental setup of the evaporation chamber for the procedure being proposed.

2. Results and Discussion

The proposed procedure consists of the following.

- 1) Previous to coevaporation, the tooling factors of both PbI_2 - and MAPbI_3 -QCMs are calibrated in relation to PbI_2 . That implies that when only PbI_2 is evaporated inside the chamber, the deposition rates from both QCMs should display identical values.
- 2) For the coevaporation, initially only PbI_2 is heated. Once its sublimation can be detected on both QCMs, the temperature of PbI_2 is fine tuned to lead to a stable sublimation rate of precisely 0.50 \AA s^{-1} on the MAPbI_3 -QCM; ideally, the rate read on the PbI_2 -QCM (X_{PbI_2}) should also be 0.50 \AA s^{-1} , but usually X_{PbI_2} can differ by $\pm 0.02 \text{ \AA s}^{-1}$ from the value read on MAPbI_3 -QCM due to experimental errors when reading with QCMs (which normally can be up to 10%). Therefore, if X_{PbI_2} is not 0.50 \AA s^{-1} , one should take note of the X_{PbI_2} value being read on the PbI_2 -QCM before proceeding to the next step.
- 3) The MAI is heated, and the MAI temperature is adjusted so that the sublimation detected on the MAPbI_3 -QCM (Y_{MAPbI_3} , equal to the initial 0.50 \AA s^{-1} from PbI_2 plus a certain amount coming from MAI) reaches a stable rate of a desired value.
- 4) The rate on the PbI_2 -QCM is then kept stable at precisely X_{PbI_2} by adjusting the PbI_2 temperature if necessary; given that this condition is followed during the whole course of coevaporation, any changes in Y_{MAPbI_3} on the MAPbI_3 -QCM should be considered to come from MAI exclusively, which then can be adjusted by tuning the MAI temperature.

To test how different MAI batches with different MAH_2PO_2 contents (i.e., 0.00, 0.03, 0.18, and 0.49 mol%) can affect the deposition control in this proposed setup, two set of experiments

were performed. In the first one (trials A), the sublimation temperature of the different MAI batches was set to the same value (95 °C) and kept constant for the duration of the evaporation process. This led to different rates at the MAPbI₃-QCM depending on the amount of MAH₂PO₂:MAI. The second experiments (trials B) consisted of setting the same evaporation rate at the MAPbI₃-QCM for all MAI batches and maintaining it constant for the duration of the evaporation process. This required setting different temperatures at the MAI source depending on the amount of MAH₂PO₂ in the particular MAI batch. The evaporation process was finished for both experiments when a targeted thickness of around 100 nm was reached at the MAPbI₃-QCM. Note that this final perovskite thickness is thinner than normally used in solar cells, that is, >500 nm; by doing so, we were able to perform all the trials, eight MAPbI₃ in total, in the same day, to maintain their evaporation and facility conditions as similar as possible. Also, a lower thickness allows for comparing small variations in the absorption of different films, hence for a better estimate about reproducibility of their optical quality, while thicker films would barely show any differences in absorption as they would absorb practically all the incident light regardless of the sample. The four different MAH₂PO₂:MAI mixtures were synthesized prior to the trials (see experimental details and Figure S1 and S2, Supporting Information).

Figures 2A–C shows variations in MAI temperature, chamber pressure, and Δ_{rate} from the MAPbI₃-QCM versus time for trial A (in which Δ_{rate} represents the deviation from the initial PbI₂'s 0.50 Å s⁻¹ rate on the MAPbI₃-QCM, standing as an indirect measure for the MAI rate). As shown in Figure 2A, the temperature of MAI was set to 95 °C and the shutter was opened when the source reached the set temperature; the shutter was closed to finish the deposition when the thickness reading at the MAPbI₃-QCM reached 100 nm. For all coevaporations with the different MAI batches, an increase in chamber pressure was detected once the MAI started to evaporate (Figure 2B), but after a few minutes, the baseline chamber pressure of 2×10^{-6} mbar was re-established. The deviation from the baseline pressure was larger for the MAI batch containing a larger amount of the MAH₂PO₂ impurity. This is indicative of degassing or decomposition of the MAI at the initial stages of evaporation, as was also observed by Borchert.^[51] From Figure 2C, it is clear that the QCM recorded a larger Δ_{rate} which means a higher MAI deposition rate for batches with larger amounts of MAH₂PO₂:MAI. When comparing the actual final thicknesses of the coevaporated films on glass substrates measured with a mechanical profilometer, thicker films were obtained for deposition using MAI batches that contained more MAH₂PO₂:MAI impurities (Figure 3B). In other words, the trend in thickness follows the trend in Δ_{rate} , indicating that the larger rates observed are caused by more MAI mass reaching the substrate. A similar observation was made by Roß and coauthors.^[18]

The deposited films from trial A were analyzed using X-ray diffraction (XRD,) profilometry, optical absorbance, and by their appearance. The samples used to analyze the XRD were deposited on N4,N4,N4'',N4''-tetra([1,1'-biphenyl]-4-yl)-[1,1':4',1''-terphenyl]-4,4''-diamine (TaTm)-coated glass substrates. This was done to ensure equal deposition conditions as that used when the perovskite layer was integrated in photovoltaic devices. The diffraction patterns obtained from XRD of the as-deposited

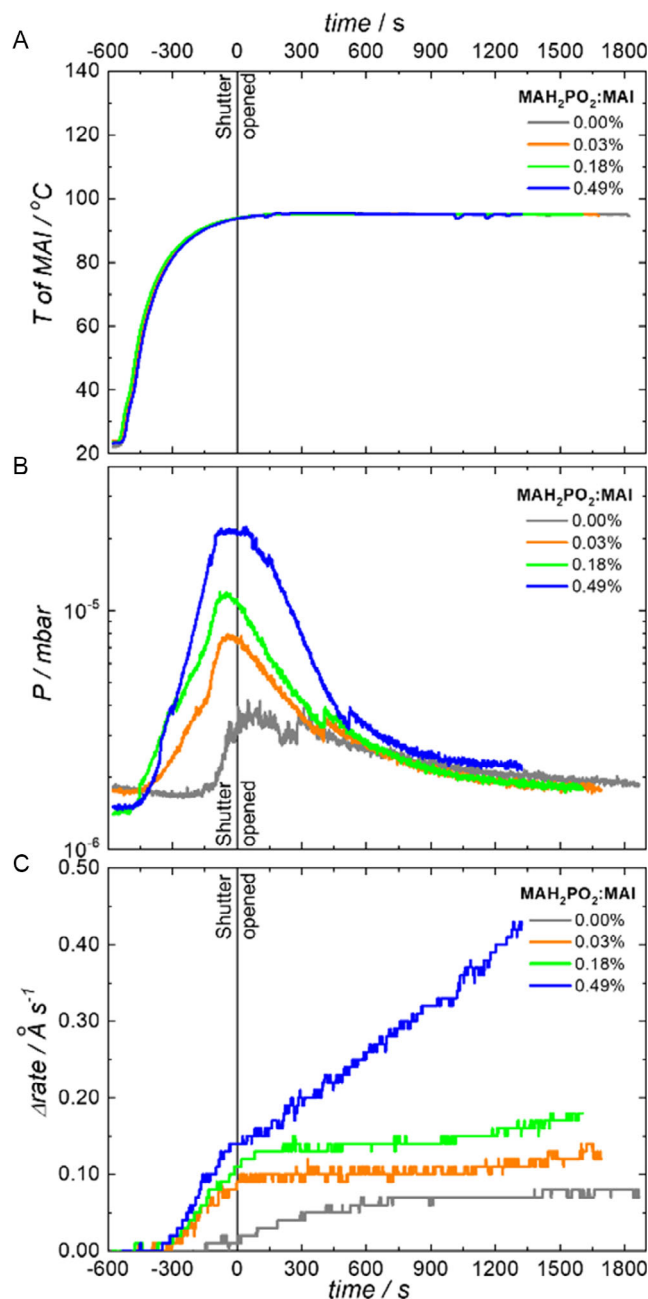


Figure 2. Variations in A) MAI temperature, B) chamber pressure, and C) Δ_{rate} in the MAPbI₃-QCM over time for trial A using MAI precursor batches with different contents of MAH₂PO₂ impurities (MAH₂PO₂:MAI = 0.00, 0.03, 0.18, and 0.49 mol%). In this trial A, the sublimation temperature of all the MAI batches was set at 95 °C.

films obtained from the different MAI batches are shown in Figure 3A.

The film deposited using the MAI batch without MAH₂PO₂ consists of MAPbI₃ with excess of PbI₂, showing PbI₂ diffraction peaks at 2θ of 12.7° and 38.6°. For samples with increasing MAH₂PO₂ concentration, as more MAI reached the substrates, the intensity of the PbI₂ diffraction peaks decreased in relation to those originating from MAPbI₃'s [110] peak at 14.1°, indicating a

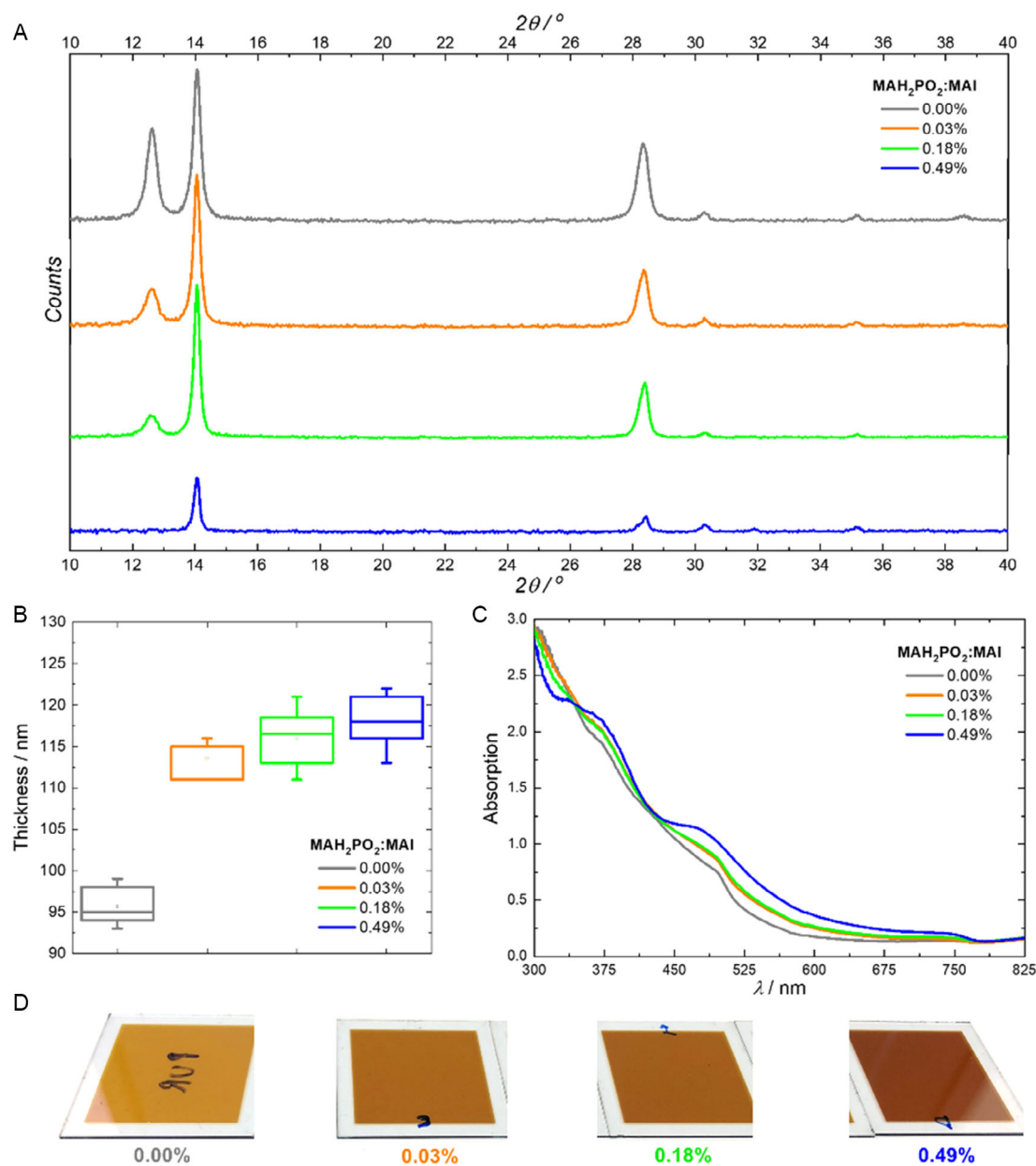


Figure 3. A) XRD patterns, B) thickness, C) absorption spectra, and D) photographs of coevaporated films as deposited in trial A using MAI precursors with different contents of MAH₂PO₂ impurities (MAH₂PO₂:MAI = 0.00, 0.03, 0.18, and 0.49 mol%).

higher degree of conversion of PbI₂ to perovskite. For the most impure MAI batch containing 0.49 mol% MAH₂PO₂:MAI, the largest amount of MAI was evaporated; hence, no residual PbI₂ was observed in the diffractogram; however, the over excess of MAI seems to be prejudicial, as the [110] peak decreased in intensity as compared to the MAPbI₃ sample formed by depositing the MAI batch with 0.18 mol% MAH₂PO₂:MAI. The MAPbI₃'s [220] peak around 28.3° also showed a shift from 28.3° to 28.4° as more MAI was evaporated for the batches containing more MAH₂PO₂:MAI (see Figure S3, Supporting Information), possibly suggesting the beginning of a change in the perovskite phase, from cubic to tetragonal.^[64]

Moreover, the absorption spectra and color tone (Figure 3C,D) of the as-deposited films also present variations, in line with the observation from XRD and layer thickness. The amount of MAPbI₃ formed increased when MAI batches with increasing amount of MAH₂PO₂:MAI were used, hence the absorption increased as did the intensity of the color of the thin films. Note that the total film thickness is less than what is usually used in photovoltaic devices, which is why they are all not strongly colored.

Therefore, the results in trial A indicate that, at a fixed applied temperature, more MAI is evaporated, the greater the concentration of MAH₂PO₂ impurity is; hence, the variations in Δ_{rate} on the MAPbI₃-QCM are real and not artefacts caused by changes in the sticking coefficient on the QCM surface. This implies that

the presence of MAH₂PO₂ in the MAI powder leads to a decrease of the vapor pressure of MAI.^[18] The different amounts of MAI reaching the substrates led to different films with different crystal and optical properties; in this sense, the final composition of the deposited MAPbI₃ varied from PbI₂-rich (less MAI reaching the substrate) to stoichiometric or MAI-rich (more MAI reaching the substrate). Obviously, using such films in PSCs will lead to differences in photovoltaic performance parameters. See how such differences in composition could affect the performance of MAPbI₃-based solar cells in Figure S4, Supporting Information; as shown in Figure S4, Supporting Information, the solar cells benefit from having a slight excess of unreacted PbI₂ in the MAPbI₃ film to boost their performance as unreacted PbI₂ can improve the crystallization of the perovskite into the cubic phase, which is more desired for efficient devices.^[64,65]

In the second experiment, trial B, Δ_{rate} was set to a stable value of $0.16 \pm 0.01 \text{ \AA s}^{-1}$ (equivalent to $Y_{\text{MAPbI}_3} = 0.66 \text{ \AA s}^{-1}$), that is, the mass of MAI reaching the MAPbI₃-QCM was controlled to be the same for all the MAI batches by adjusting the source temperature. This rate was chosen based on the Δ_{rate} values observed in trial A for MAPbI₃ deposition using MAH₂PO₂:MAI proportion of 0.18 mol%, which led to the perovskite with the most ideal XRD pattern for the highest efficiencies in PSCs. Note that we assume this value may change in other evaporator chambers as it is dependent on geometrical factors; hence, preoptimizations of Y_{MAPbI_3} would be required for all new systems applying this procedure. The shutter was opened once the target Δ_{rate} was reached, **Figure 4C**, and closed to stop the deposition when the thickness monitored at the MAPbI₃-QCM reached 100 nm. As similarly observed in trial A, an increase in chamber pressure was detected once MAI started to evaporate (Figure 4B), ascribed to degassing of molecules at the initial stages of evaporation. However, as the time required to reach the specific requirements of trial B was slightly longer than in trial A, the pressure inside the chamber already diminished back to $<3 \times 10^{-6}$ mbar, regardless of the MAH₂PO₂ concentration, when the shutter was opened (Figure 4B). Importantly, MAI batches with increasing amounts of MAH₂PO₂:MAI require lower temperatures in order to maintain the MAI rate at the substrate fixed at 0.66 \AA s^{-1} (Figure 4A). This corroborates with the above observation that the presence of MAH₂PO₂ can decrease the vapor pressure of MAI. The source temperature of the MAI source was almost constant over time once the sublimation started; hence, no adjustment in the source temperature was needed to maintain the set MAI evaporation rate. Similar remarks were also observed for longer evaporations with more than two hours of thicker perovskites (check Figure S5, Supporting Information). Note that it is possible to sublime the perovskite at higher rates too, reducing the overall deposition time, but in this study we chose to focus on control rather than speed.

As shown in **Figure 5B**, the final thicknesses of the deposited MAPbI₃ ranged from 115 to 120 nm, which can be considered equivalent. Note that this value deviates from the 100 nm measured on the MAPbI₃-QCM because the QCM is actually calibrated in relation to PbI₂ alone, as described earlier. Moreover, the perovskite XRD patterns in Figure 5A (for perovskites deposited on glass/TaTm substrates) indicated similar degree of crystal conversion and orientation, with no changes in peak shape or angles. Finally, all four perovskites deposited,

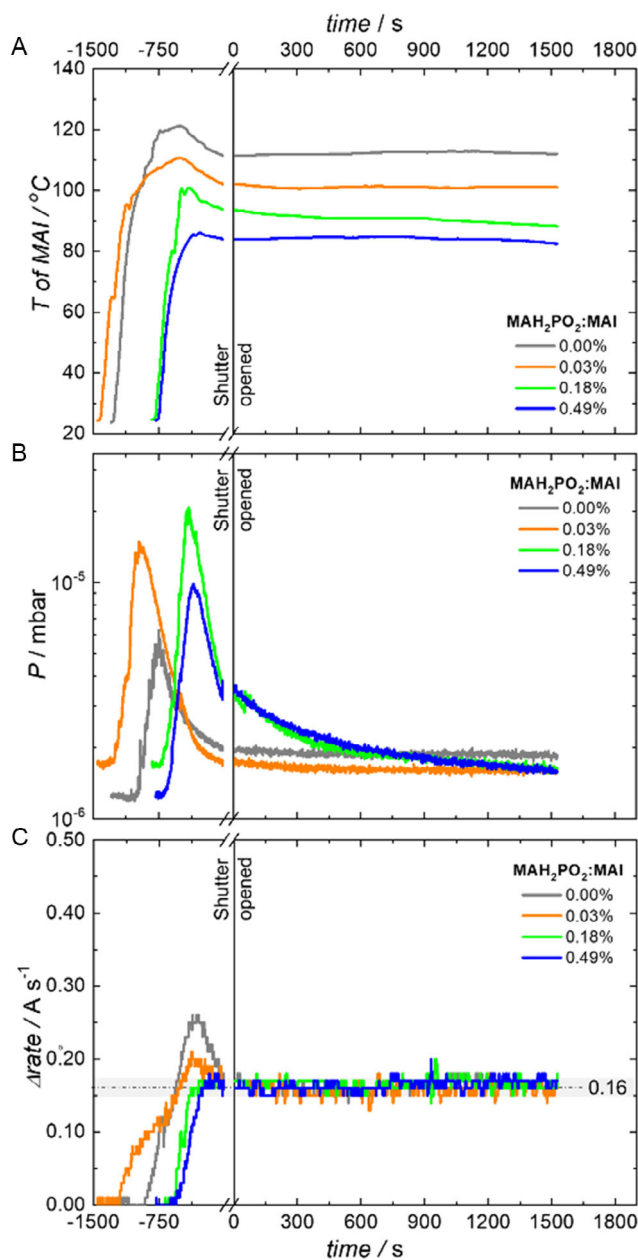


Figure 4. Variations in A) MAI temperature, B) chamber pressure, and C) Δ_{rate} in the MAPbI₃-QCM over time for trial B using MAI precursors with different contents of MAH₂PO₂ impurities (MAH₂PO₂:MAI = 0.00, 0.03, 0.18, and 0.49 mol%). In this trial B, the sublimation of different MAI samples was controlled through the MAPbI₃-QCM, fixing their Δ_{rate} to the same value (0.16 \AA s^{-1}).

regardless of the different MAH₂PO₂ contents in the sublimed MAI, exhibited the same absorbance spectra, without apparent changes in color, as exhibited in Figure 5C,D.

Therefore, the procedure proposed in trial B led to a better control of the perovskite reproducibility. This is because the perovskite growth is controlled via the total perovskite mass (or PbI₂ + MAI mass) reaching the MAPbI₃-QCM. It also proves our initial hypothesis that the sticking of MAPbI₃ on the

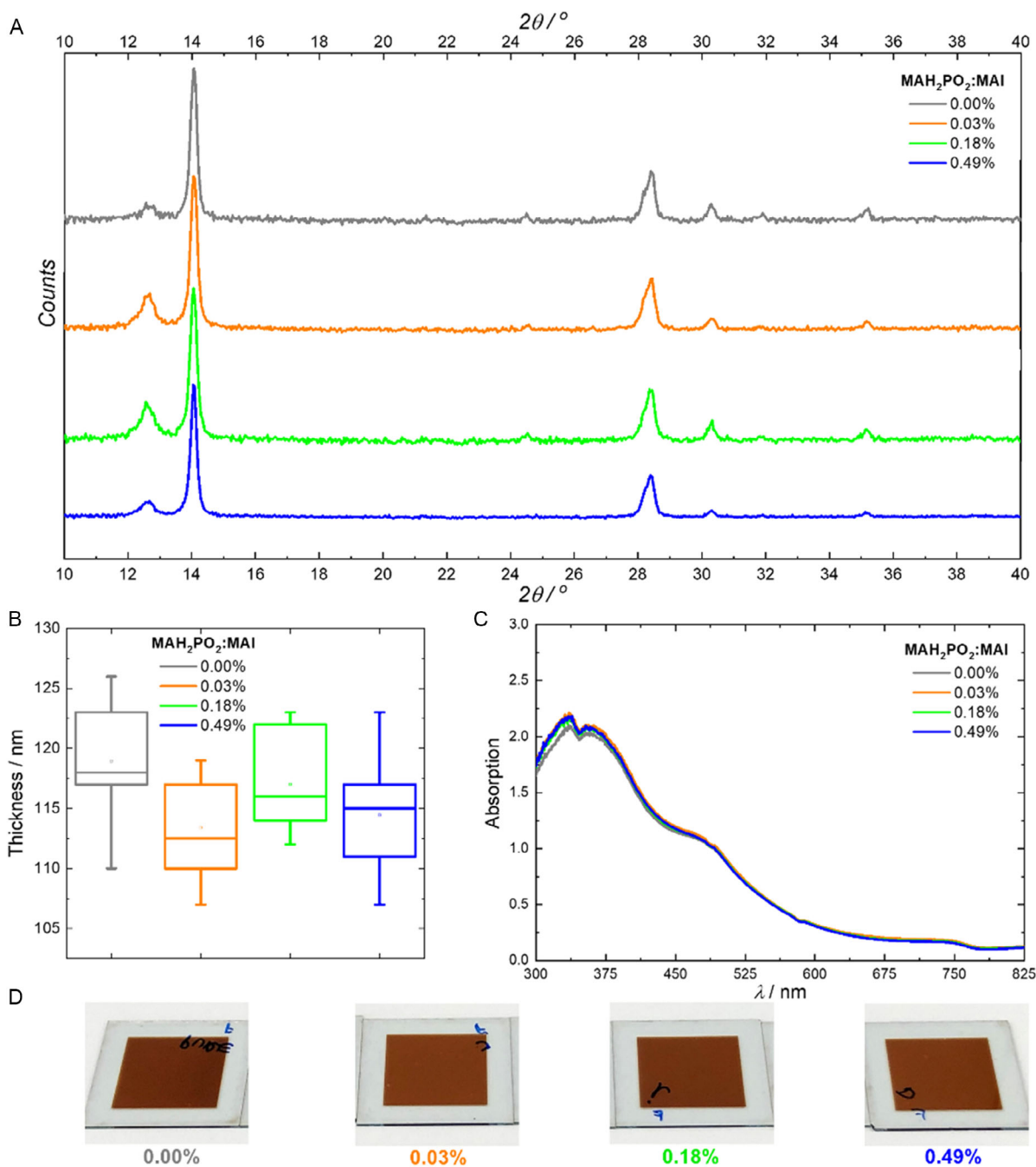


Figure 5. A) XRD, B) thickness, C) absorption spectra, and D) color of coevaporated films, as deposited in trial B using MAI precursors with different contents of MAH_2PO_2 impurities ($\text{MAH}_2\text{PO}_2:\text{MAI} = 0.00, 0.03, 0.18$ and 0.49 mol%).

QCM sensor (placed close to the substrate) is not subject to changes during the course of the evaporation, regardless of $\text{MAH}_2\text{PO}_2:\text{MAI}$.

Some of these thin perovskite films deposited from MAI with different MAH_2PO_2 contents were integrated in photovoltaic devices. For that, we selected a pin architecture with the following layer sequence, which we described elsewhere^[66]: glass/ITO (≈ 150 nm)/ MoO_3 (6 nm)/TaTm (10 nm)/ MAPbI_3 (115–120 nm)/ C_{60} (25 nm)/BCP (7 nm)/Au (see supporting information for

more details on their fabrication). The devices were encapsulated using atomic layer deposition of Al_2O_3 at 40°C , using a protocol recently published by us.^[67]

As exhibited in **Figure 6A,B**, their current density–voltage (J – V) curves, either illuminated or in the dark, are practically identical. **Figure 6C** also shows that their photovoltaic properties are statically the same, regardless of the initial amount of MAH_2PO_2 impurity in the MAI, with all samples generating open-circuit voltage (V_{OC}) of 1.11–1.12 V and short-circuit

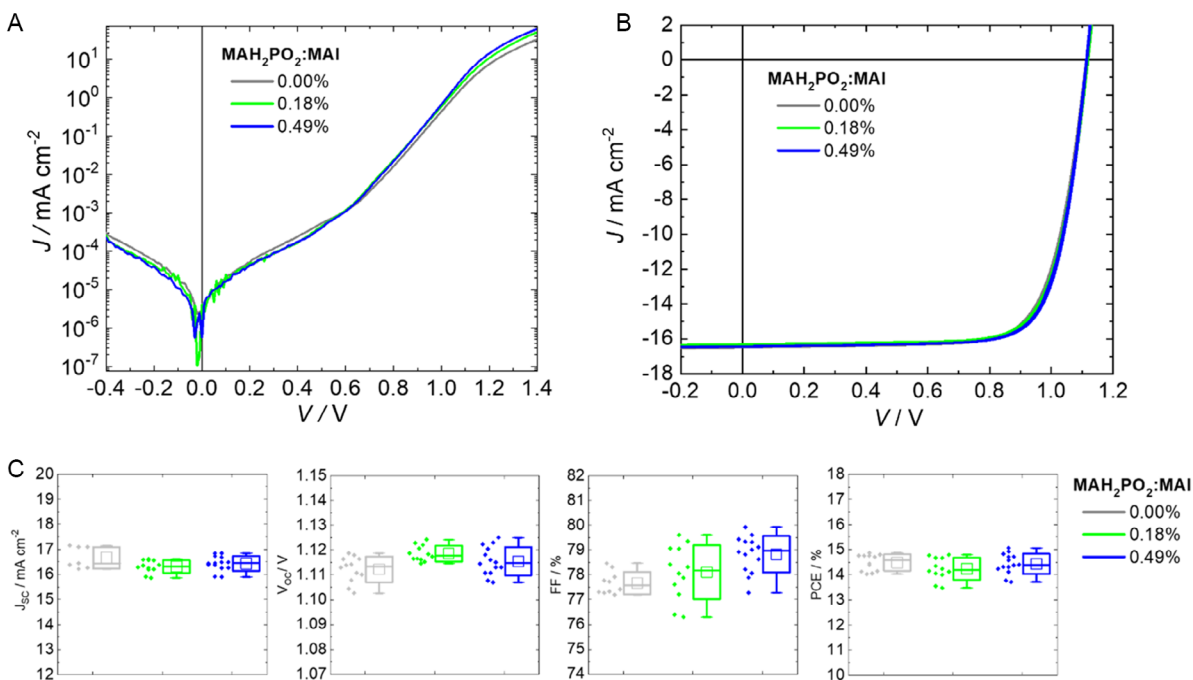


Figure 6. A) Dark and B) illuminated $J-V$ curves (measured under AM 1.5G irradiation at 100 mW cm^{-2} at room temperature) of glass/ITO/MoO₃/TaTm/MAPbI₃/C₆₀/BCP/Ag devices having the thin (120 nm) MAPbI₃ films deposited in trial B using MAI precursors with different contents of MAH₂PO₂ impurities (MAH₂PO₂:MAI = 0.00, 0.18 and 0.49 mol%). C) Statistic distribution of J_{SC} , V_{OC} , FF, and PCE.

current density (J_{SC}) of 16.5–17.0 mA cm⁻². Thus, with fill factors (FFs) of 77–79%, their final PCE is identical, ranging from 14 to 15%. Note that the perovskite films in these devices are thin (i.e., ≈ 120 nm); hence, their J_{SC} and PCE have lower values than those observed for thicker (>500 nm) MAPbI₃ films. The

external quantum efficiency (EQE) spectra are depicted in Figure S6, Supporting Information. Therefore, when the perovskite is deposited in the setup we are proposing with trial B, the performance of the devices is the same regardless of different MAH₂PO₂ impurity concentrations.

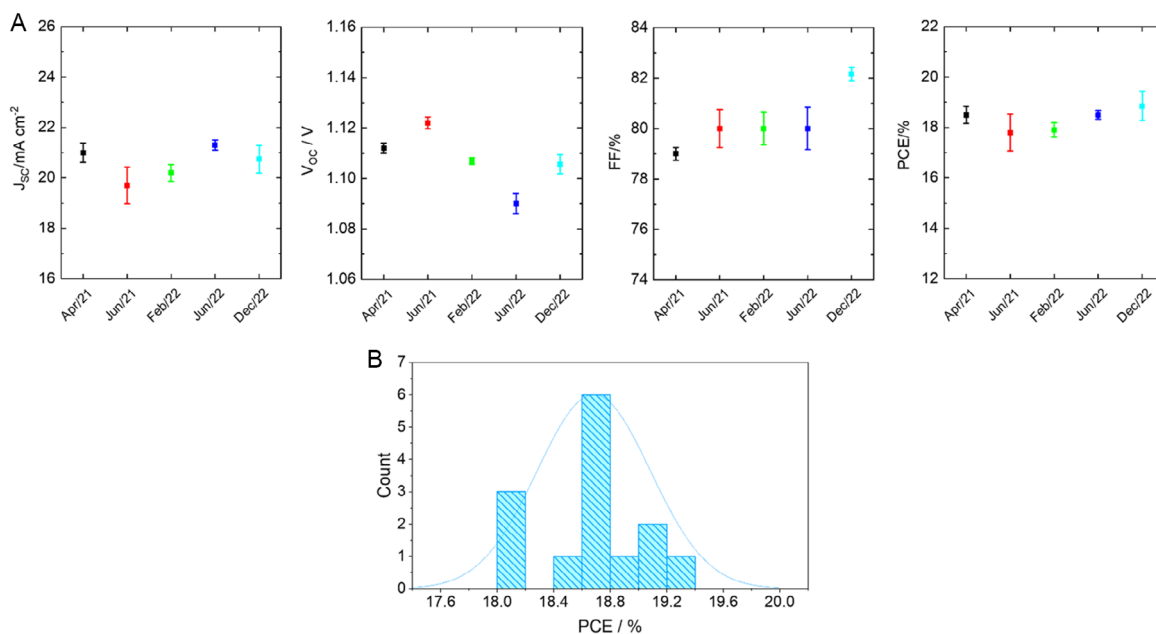


Figure 7. A) Average and standard deviation of V_{OC} , FF, J_{SC} , and PCE of MAPbI₃ devices (500 nm thick perovskites) fabricated in our laboratory using the setup of trial B with different MAI batches over the course of one and a half years. B) Histogram of the PCE of 14 samples of the batch from December 2022.

To further prove that the procedure described under trial B led to rather reproducible perovskite films over time, in **Figure 7A**, we compare the results we have been obtaining for some MAPbI₃ devices in our laboratory in the past one and a half years, since this setup was implemented. These results are for perovskite films more than 500 nm thick, deposited with different MAI batches either from different providers or with different MAH₂PO₂ mol% concentrations in the batches; for example, the MAI used on April 2021 or December 2022 was from the same provider but had around 0.2 or 0.9 mol% of MAH₂PO₂, respectively (based on ¹H NMR integrals). As summarized in **Figure 7A**, the V_{OC}, FF, and J_{SC} obtained during that time were constant, around 1.11 V, 80%, and 20.5 mA cm⁻², respectively, with some small variations related to some discrete differences in the stack configuration that affect light harvesting at the active perovskite layer (e.g., different glass/ITO substrate, CTL, or top contacts). Therefore, the PCE varied from 18 to 19% regardless of the MAI used, showing that with the setup proposed in trial B, the devices are not subject to batch-to-batch variations, enhancing reproducibility.

3. Conclusions

In conclusion, we established a new protocol for the reproducible deposition of MAPbI₃ that takes into account the total amount of MAPbI₃ mass reaching the substrates. We prove that MAPbI₃ can be evaporated reproducibly without a MAI-dedicated QCM. This procedure avoids uncertainty in the rate feedback controls, which are typically observed when monitoring MAI alone due to varying sticking coefficients, hence increasing the reproducibility of the deposited MAPbI₃. Importantly, we demonstrate through the use of four different MAI batches, each with a different amount of the known MAH₂PO₂ impurity, that virtually identical perovskites can be obtained as long as the sublimation is controlled by the deposition rate of the MAPbI₃. Moreover, using this approach, we were able to elucidate that the MAH₂PO₂ impurity leads to a reduction of the sublimation temperature of MAI.

Supporting Information

Supporting Information is available from the Wiley Online Library or from the author.

Acknowledgements

The authors gratefully acknowledge financial support of the European Research Council (ERC) under the European Union's Horizon 2020 research and innovation programme (grant agreement no. 834431). Authors acknowledge support from the Comunitat Valenciana: H.B. for projects IDIFEDER/2018/061 and PROMETEU/2020/077 and M.S. for project CISEJ/2022/43. Authors also acknowledge support by the Ministry of Science and Innovation (MCIN) and the Spanish State Research Agency (AEI): Grant PDC2021-121317-100 funded by MCIN/AEI/10.13039/501100011033 and by the "European Union NextGenerationEU/PRTR"; grants PRE2019-091181 and RYC-2016-21316 funded by MCIN/AEI/10.13039/501100011033 and by "ESF Investing in your future"; Project CEX2019-000919-M funded by MCIN/AEI/10.13039/501100011033; K.P.S.Z for a Juan de la Cierva scholarship (IJC2020-045130-I).

Conflict of Interest

The authors declare no conflict of interest.

Data Availability Statement

The data that support the findings of this study are available from the corresponding author upon reasonable request.

Keywords

methyammonium iodide, perovskite solar cells, vacuum deposition

Received: December 1, 2022

Revised: January 9, 2023

Published online: February 1, 2023

- [1] J. Jeong, M. Kim, J. Seo, H. Lu, P. Ahlawat, A. Mishra, Y. Yang, M. A. Hope, F. T. Eickemeyer, M. Kim, Y. J. Yoon, I. W. Choi, B. P. Darwich, S. J. Choi, Y. Jo, J. H. Lee, B. Walker, S. M. Zakeeruddin, L. Emsley, U. Rothlisberger, A. Hagfeldt, D. S. Kim, M. Grätzel, J. Y. Kim, *Nature* **2021**, 592, 381.
- [2] W. A. Dunlap-Shohl, Y. Zhou, N. P. Padture, D. B. Mitzi, *Chem. Rev.* **2019**, 119, 3193.
- [3] J. Burschka, N. Pellet, S.-J. Moon, R. Humphry-Baker, P. Gao, M. K. Nazeeruddin, M. Grätzel, *Nature* **2013**, 499, 316.
- [4] N. J. Jeon, J. H. Noh, Y. C. Kim, W. S. Yang, S. Ryu, S. Il Seok, *Nat. Mater.* **2014**, 13, 897.
- [5] Q. Chen, H. Zhou, Z. Hong, S. Luo, H.-S. Duan, H.-H. Wang, Y. Liu, G. Li, Y. Yang, *J. Am. Chem. Soc.* **2014**, 136, 622.
- [6] M. R. Leyden, L. K. Ono, S. R. Raga, Y. Kato, S. Wang, Y. Qi, *J. Mater. Chem. A* **2014**, 2, 18742.
- [7] Y. Peng, G. Jing, T. Cui, *J. Mater. Chem. A* **2015**, 3, 12436.
- [8] W. S. Yang, B.-W. Park, E. H. Jung, N. J. Jeon, Y. C. Kim, D. U. Lee, S. S. Shin, J. Seo, E. K. Kim, J. H. Noh, S. Il Seok, *Science* **2017**, 356, 1376.
- [9] H. Kim, K.-G. Lim, T.-W. Lee, *Energy Environ. Sci.* **2016**, 9, 12.
- [10] B. Chen, Z. J. Yu, S. Manzoor, S. Wang, W. Weigand, Z. Yu, G. Yang, Z. Ni, X. Dai, Z. C. Holman, J. Huang, *Joule* **2020**, 4, 850.
- [11] A. J. Harding, A. G. Kuba, B. E. McCandless, U. K. Das, K. D. Dobson, B. A. Ogunnaik, W. N. Shafarman, *RSC Adv.* **2020**, 10, 16125.
- [12] B.-S. Kim, L. Gil-Escrig, M. Sessolo, H. J. Bolink, *J. Phys. Chem. Lett.* **2020**, 11, 6852.
- [13] P.-S. Shen, Y.-H. Chiang, M.-H. Li, T.-F. Guo, P. Chen, *APL Mater.* **2016**, 4, 091509.
- [14] Y. Ma, Q. Zhao, *J. Energy Chem.* **2022**, 64, 538.
- [15] Y. Jiang, S. He, L. Qiu, Y. Zhao, Y. Qi, *Appl. Phys. Rev.* **2022**, 9, 021305.
- [16] S.-R. Bae, D. Y. Heo, S. Y. Kim, *Mater. Today Adv.* **2022**, 14, 100232.
- [17] Y. Yang, Z. Xue, L. Chen, C. F. J. Lau, Z. Wang, *J. Energy Chem.* **2021**, 59, 626.
- [18] M. Roß, M. B. Stutz, S. Albrecht, *Sol. RRL* **2022**, 6, 2200500.
- [19] Z. Wu, S. Bai, J. Xiang, Z. Yuan, Y. Yang, W. Cui, X. Gao, Z. Liu, Y. Jin, B. Sun, *Nanoscale* **2014**, 6, 10505.
- [20] O. Malinkiewicz, A. Yella, Y. H. Lee, G. M. Espallargas, M. Graetzel, M. K. Nazeeruddin, H. J. Bolink, *Nat. Photonics* **2014**, 8, 128.
- [21] T. Abzieher, J. A. Schwenzler, S. Moghadamzadeh, F. Sutterluti, I. M. Hossain, M. Pfau, E. Lotter, M. Hetterich, B. S. Richards, U. Lemmer, M. Powalla, U. W. Paetzold, *IEEE J. Photovoltaics* **2019**, 9, 1249.

- [22] J. Li, H. Wang, X. Y. Chin, H. A. Dewi, K. Vergeer, T. W. Goh, J. W. M. Lim, J. H. Lew, K. P. Loh, C. Soci, T. C. Sum, H. J. Bolink, N. Mathews, S. Mhaisalkar, A. Bruno, *Joule* **2020**, *4*, 1035.
- [23] H. A. Dewi, J. Li, H. Wang, B. Chaudhary, N. Mathews, S. Mhaisalkar, A. Bruno, *Adv. Funct. Mater.* **2021**, *31*, 2100557.
- [24] J. Li, H. A. Dewi, H. Wang, J. H. Lew, N. Mathews, S. Mhaisalkar, A. Bruno, *Sol. RRL* **2020**, *4*, 2000473.
- [25] J. Li, H. A. Dewi, H. Wang, J. Zhao, N. Tiwari, N. Yantara, T. Malinauskas, V. Getautis, T. J. Savenije, N. Mathews, S. Mhaisalkar, A. Bruno, *Adv. Funct. Mater.* **2021**, *31*, 2103252.
- [26] R. C. Shallcross, S. Olthof, K. Meerholz, N. R. Armstrong, *ACS Appl. Mater. Interfaces* **2019**, *11*, 32500.
- [27] L. Gil-Escrig, M. Roß, J. Sutter, A. Al-Ashouri, C. Becker, S. Albrecht, *Sol. RRL* **2021**, *5*, 2000553.
- [28] C. Gao, J. Liu, C. Liao, Q. Ye, Y. Zhang, X. He, X. Guo, J. Mei, W. Lau, *RSC Adv.* **2015**, *5*, 26175.
- [29] J. Borchert, H. Boht, W. Fränzel, R. Csuk, R. Scheer, P. Pistor, *J. Mater. Chem. A* **2015**, *3*, 19842.
- [30] L. K. Ono, M. R. Leyden, S. Wang, Y. Qi, *J. Mater. Chem. A* **2016**, *4*, 6693.
- [31] B.-S. Kim, M.-H. Choi, M.-S. Choi, J.-J. Kim, *J. Mater. Chem. A* **2016**, *4*, 5663.
- [32] C. Mombiona, L. Gil-Escrig, E. Bandiello, E. M. Hutter, M. Sessolo, K. Lederer, J. Blochwitz-Nimoth, H. J. Bolink, *Energy Environ. Sci.* **2016**, *9*, 3456.
- [33] Y. Zou, Q. Meng, H. Mao, D. Zhu, *Org. Electron.* **2017**, *41*, 307.
- [34] V. Arivazhagan, J. Xie, Z. Yang, P. Hang, M. M. Parvathi, K. Xiao, C. Cui, D. Yang, X. Yu, *Sol. Energy* **2019**, *181*, 339.
- [35] E. M. Hutter, R. J. Sutton, S. Chandrashekar, M. Abdi-Jalebi, S. D. Stranks, H. J. Snaith, T. J. Savenije, *ACS Energy Lett.* **2017**, *2*, 1901.
- [36] Y.-H. Chiang, M. Anaya, S. D. Stranks, *ACS Energy Lett.* **2020**, *5*, 2498.
- [37] A. M. Igual-Muñoz, A. Castillo, C. Dreessen, P. P. Boix, H. J. Bolink, *ACS Appl. Energy Mater.* **2020**, *3*, 2755.
- [38] I. Susic, L. Gil-Escrig, F. Palazon, M. Sessolo, H. J. Bolink, *ACS Energy Lett.* **2022**, *7*, 1355.
- [39] K. B. Lohmann, S. G. Motti, R. D. J. Oliver, A. J. Ramadan, H. C. Sansom, Q. Yuan, K. A. Elmostekawy, J. B. Patel, J. M. Ball, L. M. Herz, H. J. Snaith, M. B. Johnston, *ACS Energy Lett.* **2022**, *7*, 1903.
- [40] G. Longo, S. Mahesh, L. R. V. Buizza, A. D. Wright, A. J. Ramadan, M. Abdi-Jalebi, P. K. Nayak, L. M. Herz, H. J. Snaith, *ACS Energy Lett.* **2020**, *5*, 2200.
- [41] M. Liu, M. B. Johnston, H. J. Snaith, *Nature* **2013**, *501*, 395.
- [42] B. Abdollahi Nejad, I. M. Hossain, M. Jakoby, S. Moghadamzadeh, T. Abzieher, S. Gharibzadeh, J. A. Schwenzler, P. Nazari, F. Schackmar, D. Hauschild, L. Weinhardt, U. Lemmer, B. S. Richards, I. A. Howard, U. W. Paetzold, *Adv. Energy Mater.* **2020**, *10*, 1902583.
- [43] M. Roß, S. Severin, M. B. Stutz, P. Wagner, H. Köbler, M. Favin-Lévêque, A. Al-Ashouri, P. Korb, P. Tockhorn, A. Abate, B. Stannowski, B. Rech, S. Albrecht, *Adv. Energy Mater.* **2021**, *11*, 2101460.
- [44] M. Roß, L. Gil-Escrig, A. Al-Ashouri, P. Tockhorn, M. Jošt, B. Rech, S. Albrecht, *ACS Appl. Mater. Interfaces* **2020**, *12*, 39261.
- [45] M. M. Tavakoli, P. Yadav, D. Prochowicz, R. Tavakoli, *Sol. RRL* **2021**, *5*, 2000552.
- [46] Y. Choi, D. Koo, G. Jeong, U. Kim, H. Kim, F. Huang, H. Park, *Energy Environ. Sci.* **2022**, *15*, 3369.
- [47] W. Ke, D. Zhao, C. R. Grice, A. J. Cimaroli, G. Fang, Y. Yan, *J. Mater. Chem. A* **2015**, *3*, 23888.
- [48] D. Zhao, W. Ke, C. R. Grice, A. J. Cimaroli, X. Tan, M. Yang, R. W. Collins, H. Zhang, K. Zhu, Y. Yan, *Nano Energy* **2016**, *19*, 88.
- [49] D. P. Nenon, J. A. Christians, L. M. Wheeler, J. L. Blackburn, E. M. Sanehira, B. Dou, M. L. Olsen, K. Zhu, J. J. Berry, J. M. Luther, *Energy Environ. Sci.* **2016**, *9*, 2072.
- [50] E. J. Juarez-Perez, Z. Hawash, S. R. Raga, L. K. Ono, Y. Qi, *Energy Environ. Sci.* **2016**, *9*, 3406.
- [51] J. Borchert, I. Levchuk, L. C. Snoek, M. U. Rothmann, R. Haver, H. J. Snaith, C. J. Brabec, L. M. Herz, M. B. Johnston, *ACS Appl. Mater. Interfaces* **2019**, *11*, 28851.
- [52] L. E. Polander, P. Pahnner, M. Schwarze, M. Saalfrank, C. Koerner, K. Leo, *APL Mater.* **2014**, *2*, 081503.
- [53] L. Liu, J. A. McLeod, R. Wang, P. Shen, S. Duhm, *Appl. Phys. Lett.* **2015**, *107*, 061904.
- [54] S. Olthof, K. Meerholz, *Sci. Rep.* **2017**, *7*, 40267.
- [55] J. Emara, T. Schnier, N. Pourdavoud, T. Riedl, K. Meerholz, S. Olthof, *Adv. Mater.* **2016**, *28*, 553.
- [56] K. B. Lohmann, J. B. Patel, M. U. Rothmann, C. Q. Xia, R. D. J. Oliver, L. M. Herz, H. J. Snaith, M. B. Johnston, *ACS Energy Lett.* **2020**, *5*, 710.
- [57] C. Espinoza, F. Barría-Cáceres, F. A. Angel, *Mater. Lett.* **2022**, *321*, 132459.
- [58] L. K. Ono, S. Wang, Y. Kato, S. R. Raga, Y. Qi, *Energy Environ. Sci.* **2014**, *7*, 3989.
- [59] J. Teuscher, A. Ulianov, O. Müntener, M. Grätzel, N. Tétreault, *ChemSusChem* **2015**, *8*, 3847.
- [60] K. L. Heinze, O. Dolynchuk, T. Burwig, J. Vaghani, R. Scheer, P. Pistor, *Sci. Rep.* **2021**, *11*, 15299.
- [61] I. Levchuk, Y. Hou, M. Gruber, M. Brandl, P. Herre, X. Tang, F. Hoegl, M. Batentschuk, A. Osvet, R. Hock, W. Peukert, R. R. Tykewinski, C. J. Brabec, *Adv. Mater. Interfaces* **2016**, *3*, 1600593.
- [62] Z. Xiao, D. Wang, Q. Dong, Q. Wang, W. Wei, J. Dai, X. Zeng, J. Huang, *Energy Environ. Sci.* **2016**, *9*, 867.
- [63] B. Chen, Z. Yu, K. Liu, X. Zheng, Y. Liu, J. Shi, D. Spronk, P. N. Rudd, Z. Holman, J. Huang, *Joule* **2019**, *3*, 177.
- [64] F. Palazon, D. Pérez-del-Rey, B. Dänekamp, C. Dressen, M. Sessolo, P. P. Boix, H. J. Bolink, *Adv. Mater.* **2019**, *31*, 1902692.
- [65] C. Roldán-Carmona, P. Gratia, I. Zimmermann, G. Grancini, P. Gao, M. Graetzel, M. K. Nazeeruddin, *Energy Environ. Sci.* **2015**, *8*, 3550.
- [66] D. Pérez-del-Rey, L. Gil-Escrig, K. P. S. Zanoni, C. Dreessen, M. Sessolo, P. P. Boix, H. J. Bolink, *Chem. Mater.* **2019**, *31*, 6945.
- [67] I. C. Kaya, K. P. S. Zanoni, F. Palazon, M. Sessolo, H. Akyildiz, S. Sonmezoglu, H. J. Bolink, *Adv. Energy Sustainability Res.* **2021**, *2*, 2000065.